



Originally published as:

Lippmann-Pipke, J., Erzinger, J., Zimmer, M., Kujawa, C., Heerden, E., van Bester, A., Möller, H., Boettcher, M., Reches, Z. (2011): Geogas transport in fractured hard rock – Correlations with mining seismicity at 3.54 km depth, TauTona gold mine, South Africa. - *Applied Geochemistry*, 26, 12, 2134-2146

DOI: [10.1016/j.apgeochem.2011.07.011](https://doi.org/10.1016/j.apgeochem.2011.07.011)

Geogas transport in fractured hard rock – correlations with mining seismicity at 3.54 km depth, TauTona gold mine, South Africa

Johanna Lippmann-Pipke^{a,*}, Jörg Erzinger^b, Martin Zimmer^b, Christian Kujawa^b, Margaret Boettcher^c, Esta Van Heerden^d, Armand Bester^d, Hannes Moller^e,
Nicole A. Stroncik^{b,f} and Zeev Reches^g

^a Institute of Radiochemistry, Helmholtz Zentrum Dresden Rossendorf – Research Site Leipzig, Permoserstr. 15, 04318 Leipzig, Germany, j.lippmann-pipke@hzdr.de

^b Helmholtz-Zentrum Potsdam, Deutsches GeoForschungsZentrum, Telegrafenberg, 14473 Potsdam, Germany, erz@gfz-potsdam.de, weihei@gfz-potsdam.de, kujawa@gfz-potsdam.de

^c Department of Earth Sciences, University of New Hampshire, 56 College Rd, Durham, NH 03824, United States of America, margaret.boettcher@unh.edu

^d Department of Microbial, Biochemical and Food Biotechnology, University of the Free State, Bloemfontein 9300, South Africa, vheerde@ufs.ac.za, BesterPA@ufs.ac.za

^e Rock engineering, TauTona Gold Mine, AngloGold Ashanti, Carletonville, South Africa, JMoller@AngloGoldAshanti.com

^f Integrated Ocean Drilling Program, Texas A&M University, 1000 Discovery Drive, College Station, TX 77845, United States of America, stroncik@iodp.tamu.edu

^g School of Geology and Geophysics, Oklahoma University, 100 East Boyd Street Suite 810, Norman, OK 73019, United States of America, reches@ou.edu

Abstract

An on-site gas monitoring study has been conducted in the framework of an earthquake laboratory (the international NELSAM-DAFGAS projects) at the TauTona Gold mine, South Africa. Five boreholes up to 60 m long were drilled at 3.54 km depth inside a 25 m² cubby into the highly fractured Pretorius Fault zone and instruments for chemical and seismic monitoring installed therein. Over the span of four years sensitive gas monitoring devices were continuously improved to enable the direct observation of geogas concentration variations in the DAFGAS borehole. The major gas concentrations are constant and air-like with about 78% N₂, 21% O₂, 1% Ar. The geogas components CO₂, CH₄, He and H₂ show most interesting trends and variations on the minute-by-minute basis and significantly correlate with seismic data, while the ²²²Rn activity remains constant. Time series and cross correlation analysis allow the identification of different gas components (geogas and tunnel air) and the identification of two processes influencing the borehole gas composition: 1) pumping-induced tunnel air breakthrough through networks of initially water-saturated fault fractures; and 2) seismicity induced permeability enhancement of

fault fractures to above $\sim 5 \cdot 10^{-10}$ m². The current set-up of the gas monitoring system is sensitive enough to quantify the resulting geogas transport during periods of intense blasting activities (including recorded blasts with seismic moment $\leq 1 \cdot 10^9$ Nm, located within 1000 m of the cubby) – and, we suggest, also during induced earthquakes – a final goal of the project.

Keywords

Gas transport, fluid transport and seismicity, gas geochemistry, earthquake laboratory, gas breakthrough, mining, seismicity, DAFSAM, NELSAM

1. Introduction

Fluid transport and seismicity are interrelated. Fluids can trigger earthquakes and seismic activity can release fluids from rock formations. The study of this relationship requires direct and near-field observations at earthquake focal depths. Most previous studies that document fluid compositional changes related to seismic events have been conducted from the surface, while tapping into the focal region through deep wells or mineral and thermal springs (Bräuer et al., 2003). In a review on the interrelation of gas geochemistry and

* Corresponding author: j.lippmann-pipke@hzdr.de phone: +49(0)341 235-2455, fax:-2731

seismotectonic activity, Toutain and Baubron (1999) conclude that crustal fluids play a major role in the earthquake cycle. Toutain and Baubron also emphasize the need for further methodological improvements, including the establishment of networks to simultaneously record seismic, meteorological, and geochemical parameters. Few interdisciplinary studies have been performed in the near-field at earthquake focal depths, including deep underground laboratories in mine environments (King, 1986; Nicolaysen, 1992). These type of studies provide opportunities to directly measure and fully describe the interrelated system of fluid geochemistry, hydraulic pressure and conductivity, stress field, strain and seismic moment. The currently ongoing international and interdisciplinary DAFSAM-NELSAM¹-project profits not only from its location in the near-field at earthquake focal depth but also by its long-term character which allows a continuous improvement of technical details. The NELSAM project consists of an earthquake laboratory installed at 3.54 km depth in the producing TauTona gold mine, including an extended 3 dimensional seismic network installed in 5 boreholes that cross the highly fractured Pretorius Fault Zone (PFZ) (Reches, 2006). Technical details on the seismic equipment and on the nature of the induced earthquakes can be found in Boettcher et al. (2009) and McGarr et al. (2009). Our current article provides first results from the related DAFGAS²-project. The 42-m DAFGAS borehole crosses through the PFZ and aims to provide direct observation of seismic-induced geogas transport in the fractured hard rock system from formational fluid reservoirs into the borehole (and tunnel working) by our high sensitivity gas-monitoring device. The obtained data is correlated with the seismic signals, including the blast activities, on a minute-by-minute basis.

2. Site characteristics

2.1 Geology and site characteristics

The TauTona gold mine (meaning “great lion” in Sotho language), currently the deepest operating mine on Earth, is located about 80 km west of Johannesburg within the Western Deep Levels of the Witwatersrand Basin (AnglogoldAshanti). Due to its high gold mineralization the basin is one of the best investigated geologic areas of the world (Boone et al., 1989; de Wit et al., 1992). It is part of the Kaapvaal Craton, a stable crustal fragment from the Archaean era with very little natural seismicity. TauTona’s gold deposits are currently mined at depths of 2-3.5 km, and shafts are under construction to extend mining to below 4 km. The

shafts cross through the about 10 m wide and about 10 km long Pretorius Fault Zone (PFZ), the largest fault in the western deep area of the mine (Heesakkers et al., 2011a; Heesakkers et al., 2011b). Figure 1 illustrates the location of an approximately 25 m² cubby that was excavated particularly for the purpose of the DAFSAM-NELSAM earthquake laboratory (Reches, 2006) directly within the PFZ at 3.54 km depth. The ceiling and walls of the cubby were meshed to prevent rockfall, but are not cemented. A 220 V power supply was installed and a brick wall with a metal door protects the equipment from any interference with regular mining activities. From the well-ventilated cubby, five cored drill holes – including the DAFGAS hole - penetrate the slightly metamorphosed Precambrian sedimentary rocks of the Witwatersrand basin, which include mainly quartzite, conglomerates and mudrocks, as well as basaltic bodies. The 42 m long DAFGAS borehole is located 2 m above cubby ground, has a diameter of 7.5 cm and inclines with 25 degrees in north-north-eastern direction into the formations. The first few meters of the borehole are supported with perforated steel casing, the full length is supported with a perforated PVC casing.

The seismicity rate is highest immediately after blasting (~6 p.m. each week day and on every-other Saturday). In the two years from June 1, 2007 through May 31, 2009, each month an average of 672 earthquakes and 116 blasts in the magnitude range $-4 \leq M_w \leq 3$ were recorded within a region approximately centered on the cubby and extending 1822 m in the N-S direction, 1788 m in the E-W direction, and 900 m in the vertical direction. The determination of magnitude and location, as well as the classification of these events as earthquakes or blasts was performed at the mine by ISSI personal (Integrated Seismic System International, <http://www.issi.co.za>).

2.2 Origin of the geogases under investigation

Geogases are those gas components in the analyte whose concentrations significantly exceed those of air, which cannot be explained by any anthropogenic influence or technical artefact, and whose geologic origin has been well-documented in literature. ⁴He is the α -particle product in the decay series of the primordial nuclides U and Th. This radiogenic, highly diffusive noble gas is chemically inert and, if not trapped in mineral phases, fluid inclusions, or accumulated in ground water bodies (Andrews, 1985), it outgases into the Earth atmosphere and outer space with a certain average crustal flux rate (Torgersen and Clark, 1985). Lin et al. (2005) measured >7 mM H₂ dissolved in deep fracture water accessed in the deep Witwatersrand gold mines. H₂ can originate from a variety of geological and microbial processes. H₂ generating processes include organic

¹DAFSAM-NELSAM: Drilling Active Faults in South African Mines - Natural Earthquake Laboratory in South African Mines

²DAFGAS: Drilling Active Faults - Gas analysis

fermentation (Boone et al., 1989), serpentinization (Coveney et al., 1987; Sato et al., 1985), oxidation of Fe^{2+} bearing minerals (Stevens and McKinley, 2000), formation of FeS_2 to FeS (Drobner et al., 1990), thermo-decomposition of alkanes and carboxylic acids (Seewald, 2001), the interaction between Si-O radicals and water molecules (King, 1986; King and Lou, 1990; Kita et al., 1982), and a radiolytic origin of H_2 . Lin et al. (2006) conclude there is a radiolytic origin of the H_2 . Lin et al., (2006) site was a tectonically inactive Archaean craton setting, so we need to consider the mining induced re-activated fault system as an additional hydrogen source. Therefore, we consider a process described by King and Luo (1990) and Kita et al., (1982), who suggested Si-O radicals at fresh crack surfaces interact with H_2O and are likely H_2 sources in fault zones (Wiersberg and Erzinger, 2008). CO_2 is (after H_2O and N_2) the third most abundant gas species in geological systems (Toutain and Baubron, 1999). Natural discharges of CO_2 can have several sources (mantle, metamorphism of carbonate-bearing rocks or decomposition of organic material) and are often a mixture (Sugisaki et al., 1983). CH_4 generating processes are either thermogenic, microbial (bacterial) and/or abiotic. Microbial and abiogenic processes are the relevant ones for the deep Witwatersrand Basin (Sherwood Lollar et al., 1993; Sherwood Lollar et al., 2006; Sherwood Lollar et al., 2008; Sherwood Lollar et al., 2002) with microbial CH_4 able to effectively dominate abiotic quantities once a system, initially isolated throughout geologic time (Lippmann-Pipke et al., 2011), is opened up and invaded by microbes (Ward et al., 2004).

^{222}Rn is the only gaseous isotope of the U- and Th-decay chains and has a half-life of 3.8 days. Its occurrence in fracture fluids is proportional to that of its mother nuclide ^{226}Ra at fracture surfaces, the fracture surface to fracture aperture ratio and the residence time of the fracture fluid (Andrews et al., 1985).

3. Materials and methods

3.1. Gas analysis

In the first two years of the DAFGAS monitoring project (2007/08) the online long-term borehole analysis of the main and trace gas components was performed by means of a quadrupole mass spectrometer (QMS) Omnistar, Pfeiffer Vacuum, GSD 301 01, mass range 0-100 and a ^{222}Rn detector that were all installed inside an air conditioned box in the dedicated cubby at 118 level. Figure 1 illustrates the overall setting of the tunnel, the Pretorius Fault, the cubby, the five boreholes and the DAFGAS equipment (Figure 2 and 3). This QMS based system allowed for the identification of the relevant gas components in the borehole and quantified the typical variability of

their temporal concentrations. Unfortunately, the QMS turned out to be easily damaged in the harsh conditions underground and was not suitable for successful, long term, low-maintenance performance. Consequently, the QMS was replaced by a set of more robust gas specific sensors (Xgard Crowcon, Type 1 for H_2 and O_2 , and Li-COR, Li-820 for CO_2) able to monitor H_2 , CO_2 and O_2 with the necessary sensitivity (Figure 4). In early 2010 a final optimization turned the system into a stand-alone, low-maintenance, reliable device with significantly reduced dead gas volumes. In the technical annex the first and the final realization of the gas analytical systems (A 1.1, A 1.2), as well as the timeline of the analytical system performances (A 2, Figure 5) are described in full detail. Radon was analysed throughout the long-term on-line gas monitoring experiment by means of an alpha-meter (G-B.-H. series 1400, Gewerkschaft Brunhilde, Uetze, Germany) with a $\text{ZnS}(\text{Ag})$ -coated scintillation chamber. Atmospheric background activities amount to (2.5 ± 2.0) cpm (counts per minute), equivalent to about (0.43 ± 0.35) Bq l^{-1} . Rn data were stored in 1-min intervals.

3.2 Other DAFGAS units

Three temperature sensors (Heraeus, PT 1000, DIN 1/3 W-EYK6) are installed in the borehole at 20, 30 and 40 m depth, a fourth inside the air conditioned box. The cables of the borehole sensors are inserted inside a partially perforated plastic liner along with 1/16" stainless steel capillaries of 20, 30 and 40 m length. Perforated sections are 20-21m, 30-31m and 40-41m. The plastic liner is sealed shortly behind the perforations at 19.5m, 29.5m and 39.5m depth, so that only gas of a specific bore hole section is sampled with each capillary. The borehole opening is sealed to prevent immediate gas exchange with tunnel air.

The air pressure data in the cubby is derived on the basis of minute-by-minute measurements by means of a Honeywell SCX 30 pressure detector and stored on a data logger. Air pressure data for the two stations nearest to Carletonville, Potchefstroom (~50 km) and Klerksdorp (~100 km) from March and April 2007 is provided by the South African Weather Service (hourly data).

3.3 Seismic network and strain meter

The NELSAM-DAFSAM seismic and strain equipment complement the extensive in-mine seismic network that are operated by Integrated Seismic Systems International (ISSI) (Mendecki, 1997) and were installed with the aim of recording high-quality, broad-band, near-source seismic data and cross fault strain. Explicitly, a 110 m long strain/displacement meter fabricated at the United

States Geological Survey (USGS) was installed in and between the DAF1 and DAF2 boreholes (Figure 1). As of May 2007 through mid-2009 the NELSAM project collected high-frequency (up to 12 kHz) seismic data from nine instruments at five sites within and surrounding the Pretorius Fault Zone in TauTona mine. The devices regularly detect detailed waveforms of earthquakes with magnitude $M_w \geq -3.0$ located meters to hundreds of meters from the seismometers. Tests verified that true ground velocity were accurately obtained from both, the weak ground motion accelerometers (1500S low-noise MEMS from Colibrays with a +3.5g/-3.5g range over a frequency band from DC to 10 KHz) and from co-located geophones. The NELSAM array has recorded events as small as $M_w \approx -4$ (Boettcher et al., 2009) and thus has helped to bridge the previous gap between laboratory-derived results and “large” earthquakes in the field.

3.4 Data treatment and data reporting

The data evaluation of time series typically requires *detrending*. This is the removal of intermediate or longer-term trends from a data series and allows for the identification of shorter term patterns. Explicitly, we use 2-day-sliding mean and 10-minute-sliding mean values of air pressure data in section 4.2.1. These are the mean pressure values from the 24 hours (five minutes) before and after the respective hour (minute) of interest.

Trace gas concentrations are reported in absolute values and as air normalised concentrations. For the latter we assume air concentrations values of 0.5 ppmv H₂, 380 ppmv CO₂, 5.24 ppmv He and 2 ppmv CH₄, respectively.

He isotope ratios are typically reported in R/R_a values, with R being the ³He/⁴He of the sample and R_a the respective ratio of air of $1.36 \cdot 10^{-6}$ (Figure 6). Consequently, R/R_a values of 1 identify the He in a sample to originate from air, and R/R_a values below 1 indicate that radiogenic ⁴He is contributing to the He in the sample with ⁴He being the α particle of the U and Th decay series (Andrews, 1985).

4. Results and discussion

In the following sections our monitoring results from 2007 through 2010 are presented in detail along with air pressure data from the SA Weather service and seismic moment and strain measurement results from NELSAM. We start with unravelling the complex nature of the subsurface fluid system by separately discussing pressure, temperature and gas composition time series and identifying gas breakthrough effects (section 4.1). We then demonstrate the cross-correlation between seismic activity and geogas transport in the fracture networks (section 4.2).

4.1 Unravelling the subsurface fluid system by long term-monitoring

4.1.1 Surface and subsurface air pressure

Three-week mean air pressure

Air pressure data from the two nearest SA Weather Service stations, Potchefstroom and Klerksdorp, resulted in very similar overall characteristics. The three-week-mean air pressure and standard deviation of the closer station Potchefstroom (days 64-70, 19.03.-08.04.2007) amounts to (868 ± 3) mbar. In comparison the mean subsurface air pressure data and standard deviation from the same three-week interval (weekdays only) amounts to (1130 ± 5) mbar. This offset between surface and subsurface mean pressure is explained mostly with the help of the barometric formula

$$p = p_0 \cdot e^{-\Delta h/h_s} \quad (1)$$

Here p_0 denotes the mean surface air pressure of 868 mbar, Δh the vertical height between the cubby (~ 1871 m b.s.l.) and the Potchefstroom weather station (~ 1349 m o.s.l.) of ~ 3200 m, and h_s the scale height of the troposphere of ~ 8400 m. With eq. (1) the calculated mean air pressure in the cubby results in $p = (1270 \pm 30)$ mbar. The remaining difference between the calculated and the measured mean subsurface pressure of ~ 140 mbar is interpreted as due to the ventilation of the mine in under pressure mode.

Detrended hourly mean air pressure

Air pressure data from Potchefstroom and from the cubby from seven consecutive days (days 71-77, 26.03.-01.04.07) is detrended by subtracting the 2-day sliding mean value from the sliding hourly mean. The two data series show very similar daily patterns. Explicitly, the pressure starts rising in the late mornings, reaches a daily maximum before noon and drops for the daily minimum in the evening. The cross correlation between the detrended surface air pressure (Potchefstroom, hourly data minus the 2-day sliding mean) and the detrended subsurface air pressure (TauTona, 10-minute mean minus 2-day sliding mean) revealed values of 0.70 at lag 0 hours, 0.54 at 24 hours and 0.48 at 48 hours. These values reflect the strong correlation between the surface and the subsurface pressure data and imply that the ultimate cause of the typical daily air pressure changes in the subsurface is the surface meteorology.

The different typical amplitudes of the pressure variations on weekdays on surface and in the subsurface are explained by the barometric effect (eq. 1), as are the long-term mean pressure values. In contrast on Sundays the subsurface data show significant short-term variations with typical amplitudes of +17 mbar and -6 mbar from the daily mean value within a couple of hours that do not correspond to peaks at the surface. We suggest

these large subsurface pressure amplitudes are due to changing mine-air ventilation settings.

4.1.2 Borehole temperature

Borehole temperature, measured at 20, 30 and 40 m depth increased slowly from initial values of 45, 47 and 50°C by about 0.8°C/year to finally level out in the third year (2009) at 47.5, 48.8 and 52.2°C. The borehole temperature ranges between the temperature of the tunnel air ($\leq 38^\circ\text{C}$) and that of the formation ($\sim 55^\circ\text{C}$). For later calculations we consider an average borehole temperature of $50.0 \pm 0.5^\circ\text{C}$.

4.1.3 Borehole gas composition

Long-term trend of weekly mean concentrations

The concentrations of the major gas components N_2 , O_2 and Ar are constant throughout the overall monitoring experiment and, as expected, are air-like constituting about 78%, 21% and 1%, respectively. In contrast, the trace gas components CO_2 , CH_4 , He and H_2 show interesting trends and variations. First, the long-term trends of the trace gas components are discussed on the basis of daily mean baseline concentrations.

Generally, the observed concentrations of all trace gas components are significantly enhanced throughout the observation period compared to their concentrations in air. In Table 1 the daily baseline concentrations of H_2 , CO_2 , He and CH_4 and their weekly means from a total of 29 weeks from 2007, 2009 and 2010 are listed in columns 11-17, and column 18, respectively. During the first three weeks of the monitoring experiment (with day 1 = Monday, January 15th, 2007), the weekly mean concentrations increase from 149 to 167 ppmv H_2 , from 800 to 823 ppmv CO_2 , from 213 to 265 ppmv He and 1601 to 1844 ppmv CH_4 , respectively. In Figure 6 air normalised concentrations are plotted versus time in order to demonstrate the significance of the trace gas admixture to the otherwise air-like borehole gas. For the following 6 weeks no QMS data was available, though the pump kept withdrawing borehole gas at the constant rate of 2 L h^{-1} . In the 9th week of the experiment (day 63 ff) the air normalised concentrations show somewhat lower but still comparable values to the results observed prior to the QMS-breakdown. On day 68 a sudden and significant drop of all trace gas concentrations is observed (Figure 6). The air normalised daily mean He concentration drops most significantly by a factor of 11, followed by those of CH_4 , H_2 and CO_2 . Coincidentally a sudden rise of O_2 is observed from 20.3 vol.% to 20.8 vol.% (not shown). Since then, the air normalized daily baseline values of He and CH_4 continue declining gradually until the end of the 2007 observation period to values of 1.1 and 60, respectively, while the respective air

normalized values for CO_2 and H_2 level out around 50 and 1.4.

Technical improvements regarding gas analysis

Typical H_2 and CO_2 concentrations results obtained by the first (QMS-based) and the final (sensor based) gas analytical devices are displayed in Figure 7 for comparison. Please note, the QMS- and the sensor-based data originate from different time intervals. The comparison reveals the following features: (i) The QMS data show two broad CO_2 peaks each weekday, around mid-day and in the afternoon. The sensor based CO_2 data reveals two strikingly different types of peaks each weekday, a broad mid-day CO_2 peak and very sharp ones in the afternoon. (ii) The gas sensor-based system resolves much sharper H_2 peaks than the QMS-based system. (iii) The QMS data show a baseline rise and decline throughout the course of the weeks (Table 1, columns 11-17, in 2007), whereas the sensor-based data do not. Observations (i) and (ii) can be explained by a significantly larger dead volume of the QMS-based analytical system in comparison to the sensor-based one. The observation of (iii), the mid-week baseline maxima, which is not observed in the 2010 data series, could also have a simple explanation: More effective mine ventilation in close vicinity of the cubby in 2010 than in 2007.

We do not discuss in detail the continuous long-term He, CH_4 , N_2 , O_2 and Ar time series obtained by the QMS in this paper, but we point out that the wide mass range of the QMS enabled us to understand the complexity of the processes affecting the fluid system in the borehole and neighbouring fracture network.

Simultaneous occurrence of sharp geogas peaks

The occurrences of the sharp geogas peaks are summarized in Table 1, columns 4–10. On Sundays sharp geogas peaks are not observed. Whenever data is available, the number of the observed (sharp) CO_2 , H_2 , CH_4 and He peaks is identical on all days.

The cross-correlation between the sharp H_2 and the CO_2 concentration peaks was analysed on the data displayed in Figure 7. For H_2 concentrations exceeding 90 ppmv the concentration gradients were calculated and compared to those of the respective CO_2 gradients. A correlation factor of 0.38 (and a technically caused lagging of 3 minutes of the CO_2 peak after the H_2 peak) documents the simultaneous occurrence of the two sharp geogas peaks.

For He the sensitivity to detect the daily sharp peaks got lost after the final gas breakthrough on March 24th, 2007 (see 4.1.4). Sharp CH_4 peaks could be identified beyond the final tunnel air break-through (until mid-April). The last column of Table 1 lists the weekly maximum 'peak height

over baseline' value of each trace gas component. For He and CH₄ these *signal to baseline ratios* decline from initial values of 3.3 % and 1.9 % to below detection limit at about 1 % in the course of the first couple of months. In contrast, for H₂ and CO₂ these *signal to baseline ratios* increase from ~6 % and <1 % throughout the years to around 70 % and >5 %, indicating that the significance of the peaks clearly increases with declining baseline levels.

²²²Rn results

Throughout the observation period the weekly mean ²²²Rn activity in the borehole gas remained approximately constant at values varying around $2.8 \pm 0.4 \text{ Bq l}^{-1}$. In holiday seasons it increases up to 7 Bq l^{-1} , both values are typical for *soil air*. Statistical and cross-correlation data analysis did not uncover any systematic variations around these long-term mean values other than random noise. Explicitly, we did not observe any correlation of the ²²²Rn activity with the occurrences of the sharp geogas peaks of He, CO₂, H₂ and CH₄. We suggest that the observed ²²²Rn content in the borehole represents the activity level of the tunnel air and that the ²²²Rn activity level of the geogas reservoir is always equal or lower than that in the tunnel air. The fundamental difference between ²²²Rn and the other geogases is the fact that the latter can accumulate over time in a gas reservoir after they are released from a rock matrix, while ²²²Rn cannot accumulate due to its short half-life. The absence of ²²²Rn peaks is a clear indication that the processes that trigger the geogas flux into the borehole do not dominantly trigger the *release* of new geogas from minerals and rocks into the borehole, but only trigger *the transport* of accumulated geogases from proximate voids into the borehole.

The higher ²²²Rn activity in the tunnels than in the geogas reservoirs further indicates that the ventilation system effectively passes air through the subsurface working areas where fresh rock surfaces emit ²²²Rn with likely significantly larger flux rates than in the "inactive" fault fractures that access the geogas reservoir.

Origin of mid-day CO₂ peak

The shape of the mid-day CO₂ peak (the first of the daily CO₂ peaks Figure 7, bottom), which lasted about 6-8 hours, remained quite broad when it was measured with the final sensor setup of the gas analytical system. As the mid-day CO₂ peak showed up only after the final breakthrough of tunnel air (see 4.1.4) we suggest CO₂ inflows from the tunnel through the network of fracture into the borehole. However we argue against a primarily meteorological cause (and therefore the midday air pressure peak). First, the daily O₂ concentration variations in the atmosphere are characterized by

one early morning peak around 4 a.m. (Pérez et al., 2009), while we observed the mid-day CO₂ peak ~8 hours later. Second, the daily CO₂ maxima in autumn amounts to 5-25 ppmv (Pérez et al., 2009), while we observed peak maxima of 50-55 ppmv. We conclude that the mid-day CO₂ peak is due to mine related activities, including the respiration of the workers, exhausts of the machines and outgassing of the formations during and after the main shifts.

4.1.4 Air breakthrough and fracture permeability Gas withdrawal and air breakthrough

Two observations deserve an explanation: (a) The initial rise of the geogas concentrations throughout the first three-weeks of the monitoring experiment (Figure 6) was followed by (b) a series of short, abrupt geogas concentration drops (not shown except for the last and final drop in figure 6) that recovered quickly to the previous levels. We interpret observation (a) as due to the replenishment of a significant inflow of geogases from proximate reservoirs into the borehole. This implies that the fracture gas permeability between these proximate gas reservoir(s) and the borehole was initially higher than that between the borehole and the tunnel (for likely fracture orientation see Figure 1). With time the pumping of borehole gas must have exploited this easily accessible geogas reservoir causing the pressure gradient between the borehole and the tunnel to increase. Observation (b) can then be explained by the build-up of a certain critical pressure gradient, P_c , causing a tunnel air breakthrough for the temporary pressure compensation between tunnel and borehole observable by simultaneous, temporary and significant drops of all geogas concentrations. After pressure compensation, residual water from dead end pores might have again clogged the fractures due to capillary forces and the surface tension of water (Figure 8). Each gas breakthrough must have dragged along with water from the fracture network. This would coincide with our ongoing troubles with burned through filaments of the QMS caused by liquid water.

With time these tunnel air break-through events became more frequent (1st event at the third day, 2nd event at the sixth day, further four events in the course of the first week, 19 and 48 times in the second and third week) and the trace gas concentration baselines in the borehole exhibited a sustained decline. Finally on day 68 (March 24th, 2007) an effective short-circuit between the borehole and the tunnel must have finally opened up and permanently remained open since. This was demonstrated by measurements in March 2010, as the results of the composition and timely behaviour of the tunnel air (cubby air) and the borehole gas were found to be virtually identical.

Fracture permeability

As a plausibility check the fracture gas permeability κ can be estimated from the break through events and the pump rate. Initially the hydraulic conductivity of the fractures connecting the borehole with the tunnel must have been lower than those accessing the proximate geogas reservoirs. At the time of the first tunnel air breakthrough the easily accessible, proximate geogas reservoirs must have been gradually exploited and the pressure difference between the borehole and the tunnel must have reached a breakthrough capillary pressure P_c . A resulting temporary Darcy flow Q [$\text{m}^3 \text{s}^{-1}$] allowed for pressure compensation between the tunnel air and the borehole

$$Q = \kappa \cdot A / \mu \cdot P_c / L \quad (2)$$

with κ the fracture gas permeability [m^2], A the area normal to gas flow [m^2], μ the dynamic viscosity of air at 50°C of $2 \cdot 10^{-5} \text{kg m}^{-1} \text{s}^{-1}$, and $L = 5 \text{ m}$ the distance between the borehole and the tunnel. The earliest gas breakthrough event occurred after about 48 hours pump time (2 L h^{-1}) and lasted for about 80 minutes resulting in a maximal pressure difference ΔP at that time of $\sim 560 \text{ mbar}$ or $56\,000 \text{ kg m}^{-1} \text{s}^{-2}$. Considering pressure compensation during the first breakthrough event, Q amounts to about $2 \cdot 10^{-5} \text{ m}^3 \text{s}^{-1}$ (96 L in 80 minutes) with a maximal pressure difference ΔP at that time of $\sim 560 \text{ mbar}$. Until the time of the final gas break through at day 68, a total of 3264 L water vapour saturated gas ($83 \text{ g H}_2\text{O m}^{-3}$ at 50°C) had been withdrawn from the borehole and been replenished through the fracture network. The corresponding amount of water amounts to a volume V of $\sim 270 \text{ cm}^3$ initially water saturated fracture aperture that is now void (Figure 8b). Dividing this volume V by the distance between the borehole and the tunnel L , the area normal to gas flow, A , estimates to 0.54 m^2 . With eq. 2 and the above discussed parameter values the fracture permeability for gas κ amounts to $\sim 5 \cdot 10^{-10} \text{ m}^2$, a value typical for highly fractured hard rock formations (Bear, 1972).

The breakthrough critical pressure P_c reduces as the fractures between the borehole and the tunnel become more and more undersaturated. This results in increasingly frequent tunnel air breakthrough events, as observed, and the Darcy flow rate Q subsequently levelling out at about the pump rate of $5.6 \cdot 10^{-7} \text{ m}^3 \text{s}^{-1}$ or 2 L h^{-1} , respectively.

4.1.5 Noble gas isotope composition of borehole gas

In agreement with the air-like composition of the borehole gas in respect to its main components N_2 , O_2 and Ar , the $^{40}\text{Ar}/^{36}\text{Ar}$ ratio of four borehole gas samples taken during the first five months of the

experiment for off-line noble gas analysis is identical to the atmospheric value of about 295 (Table 2). In contrast, the $^3\text{He}/^4\text{He}$ and the $^4\text{He}/^{40}\text{Ar}$ ratios show significant changes throughout this period. At day 3 of the experiment the origin of He in the borehole gas is still dominated by air with an R/R_a value of 0.69. Five weeks later – but still before the final air break through (day 43) – the He in the borehole gas is 99% radiogenic in origin (smallest observed R/R_a value of 0.01). Significant amounts of He from the geogas reservoir must have replaced the initially air like He isotope ratio. The latter two samples represent the borehole gas composition after the final gas breakthrough (days 78 and 120) with R/R_a values that gradually re-approach air-like values. The ^4He concentrations and the $^4\text{He}/^{40}\text{Ar}$ co-vary consistently: These long-term trends of the isotope data support the above mentioned interpretation, that during the first couple of weeks the borehole was dominantly replenished by gases from proximate geogas reservoirs with a remarkable ^4He concentration, allowing tunnel air to break through into the borehole only sporadically. The final and permanent breakthrough of tunnel air (day 68) caused the steep drop of the ^4He concentration and the rise of the R/R_a value. Table 2 additionally provides noble gas data from a pore water sample from the DAFBIO core (TauTona, TT118), from fluid inclusions of that bulk core material and from vein quartz samples from the neighbouring Mponeng mine (Lippmann-Pipke et al., 2011). The noble gas concentrations observed in the pore water and fluid inclusions (with R/R_a values ~ 0.01 , up to $4.9 \cdot 10^{-5} \text{ cc}^4\text{He g}^{-1}_{\text{rock}}$ and $^4\text{He}/^{40}\text{Ar}$ ranging as high as $16.4 \cdot 10^6$) are suggested radiogenic end-members that admix as *geogas* component into the underground workings.

4.1.6 Geologic origin of the trace gas components

The geologic origin of the elevated He concentrations in the borehole gas is confirmed by the radiogenic R/R_a value of as low as 0.01 (section 4.1.5). The geologic origin of other trace gas components H_2 , CO_2 and CH_4 is confirmed by their significant correlation with He on the long term as well as on the minute-by-minute-basis. We suggest they are jointly transported from proximate voids typically during seismic events where they have been accumulated for significantly longer time than some half-lives of ^{222}Rn . Explicitly, we rule out the option that they were originating from explosives or steel corrosion processes. Only the mid-day CO_2 peak, as mentioned already in section 4.1.3, is suggested to be of anthropogenic origin.

4.2. Constraining the seismic induced geogas transport

4.2.1 Typical features of the seismic activity

In Figure 9 the seismic moment and the cumulative seismic moment throughout a typical week in 2009 is displayed. This figure illustrates the typical daily seismicity patterns: 1-2 clusters of small events, each with seismic moment $\leq 10^9$ Nm, typically occur shortly after noon (with little effect on the cumulative seismic moment) followed by a cluster of events, each with seismic moment of $\leq 2 \cdot 10^{10}$ Nm, at ~6 p.m. on every weekday and on every-other Saturday. The latter cluster includes larger seismic events and thus significantly affects the cumulative seismic moment release. The blasting activities shortly after noon are related to the optimized alignment of the drillhole-explosives for the primary blasting around 6 p.m, which lasts for about half an hour. Individual larger earthquakes, for example a $4.2 \cdot 10^{12}$ Nm event that occurred about 1 km from the cubby, significantly enhances the cumulative seismic moment, too (circled dot #1 in Figure 9). In our comparison of the cumulative seismic moment release with geogas data sets we aim to identify relevant distances, directions and magnitudes of seismic events capable of enhancing the PFZ fracture permeability and thus increasing the geogas concentrations above background levels.

4.2.2 Cross-correlation between geogas transport and seismic activity

A comparison of the timing of the very sharp CO₂ and H₂ geogas peaks (Figure 10, top and centre, 10.-16.05.2010) with a week of seismic data (Figure 10, bottom, 25.-31.05.2009) clearly suggests the sharp geogas peaks to be blasting induced. Unfortunately, quantitative cross-correlation analysis of the timing of the geogas peaks and the seismic activity is not possible, as well-recorded geogas data and seismic data are not available from same weeks (see Figure 5). Still, the multiple short periods a day with intensive blasting activities are typical for the underground workings on weekdays and these characteristics are clearly reflected by sharp CO₂ and H₂ geogas peaks.

Obviously, the final setup of the gas analytical system is sensitive enough to monitor gas concentration variations caused also by clusters of seismic event smaller or equal to $1 \cdot 10^9$ Nm. Certainly, explicit cross-correlations between individual seismic events and its effect on the fracture permeability inducing significant geogas inflow into the otherwise inactive fault system, and the identification of relevant distances of events to the cubby and their magnitudes can only be performed once the highest quality seismic and gas data sets are available for the same time interval. Currently, only the ISSI system is up and running, but we are positive, that our gas analytical system is now performing with the necessary accuracy, precision and reliability to wait for the NELSAM

seismic network to be re-activated allowing for minute-by-minute cross-correlation highest geogas and highest seismic data analysis.

4.2.3 Fracture permeability enhancement during seismic events

We interpret the *isochronal* occurrence of the trace gas peaks on weekdays and their timely correlation with the blasting periods as due to advective geogas transport from the formational reservoirs (proximate voids in the highly fractured PFZ) into the borehole, into the cubby and into the tunnel air. The blast seismic effect must cause pre-existing fractures in the Pretorius Fault to become temporarily more permeable than those shortcutting the borehole with the tunnel with a permeability κ of $5 \cdot 10^{-10}$ m² allowing for the enhanced geogas flux. We back up this interpretation by results of the strain measurements across the PFZ (for location of the 110 m strainmeter in DAF1 and DAF2 see Figure 1). The cross-fault strain significantly increases during the blasts by 1.2 to 3 microstrain and falls back to almost initial values thereafter. The long term effect on the Fault fracture geometry results in 98 microstrain per year (Johnston, 2009). Such blast-induced changes in rock permeability were already reported elsewhere, though not backed up with strain measurements (Gascoyne and Thomas, 1997; Nivin et al., 2001).

5. Summary and Conclusions

We achieved the primary aim of the DAFGAS project, the quantification of gases released during and after mining induced seismic events. This was accomplished by continuously improving the experimental setups in TauTona mine, by overcoming numerous technical problems, continuous improvements of the analytical system throughout years, exhaustive time series analysis of all measured parameters, the interpretation of the systematic variations by cross-correlation analysis and plausibility considerations.

Striking features of the long-term, on-site gas monitoring study in the deep TauTona gold mine are the correlated variations of geogas concentrations in the borehole gas with the blasting induced seismicity, and the quantification of the PFZ fracture gas permeability during non-blasting hours of $5 \cdot 10^{-10}$ m², and comparatively enhanced fracture gas permeability during clusters of blasting induced $\leq 10^9$ Nm seismic moment release events.

Further detailed cross-correlation analysis between geogas fluxes, fracture permeabilities and seismicity will be conducted once seismic data from the NELSAM equipment becomes available again. Then, we will aim to quantify the impact of induced earthquakes on gas transport rates and enhanced fracture permeabilities of fault zones at focal depth.

Acknowledgements

This study was supported by grants from the German Science Foundation (Deutsche Forschungsgemeinschaft) to J.L.P. (Li872/2 and /3), the Deutsches GeoForschungsZentrum Potsdam Germany and by grants from the Natural Science Foundation of the United States of America to Z.R. (EAR0409605). We would like to thank Gerrie van Aswegen, Talita Bacon, Michelle Rodel and Mari Gerenger of ISS International to overcome logistical problems and for their help with providing the seismic data from TauTona. Thanks to AngloGold Ashanti for the permission to use the TauTona mine data for this publication. We thank the South African Weather Service (www.weathersa.co.za) for providing air pressure data from the two surface stations Potchefstroom and Klerksdorp, both close to Carletonville. For their constructive comments on the manuscript we like to thank reviewers, J. Heinicke and G. Martinelli and the associate editor, L. Aquilina.

References

- Andrews, J.N., 1985. The isotopic composition of radiogenic helium and its use to study groundwater movement in confined aquifers. *Chem. Geol.*, 49: 339-351.
- Andrews, J.N., Goldbrunner, J.E., Darling, W.G., Hooker, P.J., Wilson, G.B., Youngman, M.J., Eichinger, L., Rauert, W. and Stichler, W., 1985. A radiochemical, hydrochemical and dissolved gas study of ground waters in the Molasse basin of Upper Austria. *Earth Planet. Sci. Lett.*, 73: 317-332.
- Bear, J., 1972. *Dynamics of Fluids in Porous Material*. Elsevier, New York.
- Boettcher, M.S., McGarr, A. and Johnston, M., 2009. Extension of Gutenberg-Richter distribution to MW -1.3, no lower limit in sight. *Geophys. Res. Lett.*, 36: L10307.
- Boone, D.R., Johnson, R.L. and Liu, Y., 1989. Diffusion of the interspecies electron carrier H₂ and formate in methanogenic ecosystems and its implication in the measurement of Km for H₂ or formate uptake. *Appl. Environ. Microbiol.*, 55(1735-1741).
- Bräuer, K., Kämpf, H., Strauch, G. and Weise, S.M., 2003. Isotopic evidence (³He/⁴He, ¹³C/¹²C) of fluid-triggered intraplate seismicity. *J. Geophys. Res.*, 108(B2): 2070.
- Coveney, R.M., Goebel, E.D., Zeller, E.J. and Angino, E.E., 1987. Serpentinization and the origin of hydrogen gas in Kansas. *AAPG Bull.*, 71: 39-48.
- de Wit, M.J., de Ronde, C.E.J., Tredoux, M., Roering, C., Hart, R.J., Armstrong, R.A., Green, R.W.E., Peberdy, E. and Hart, R.A., 1992. Formation of an Archaean continent. *Nature*, 357(6379): 553-562.
- Drobner, E., Huber, H., Wächtershauser, G., Rose, d. and Stetter, K.O., 1990. Pyrit formation linked with hydrogen evolution under anaerobic conditions. *Nature (London)*, 346: 742-744.
- Gascoyne, M. and Thomas, D.A., 1997. Impact of blasting on groundwater composition in a fracture in Canada's underground research laboratory. *J. Geophys. Res.*, 102(B1): 573-584.
- Heesakkers, V., Murphy, S., Lockner, D.A. and Reches, Z., 2011a. Earthquake Rupture at Focal Depth, Part II: Mechanics of the 2004 M2.2 Earthquake Along the Pretorius Fault, Tautona mine, South Africa. *Pure and Applied Geophysics*: accepted in 2011.
- Heesakkers, V., Murphy, S. and Reches, Z., 2011b. Earthquake Rupture at Focal Depth, Part I: Structure and rupture of the Pretorius Fault, TauTona Mine, South Africa. *Pure and Applied Geophysics*: accepted in 2011.
- Hildenbrand, A., Schlömer, S., Krooss, B.M. and Littke, R., 2004. Gas breakthrough experiments on pelitic rocks: comparative study with N₂, CO₂ and CH₄. *Geofluids*, 4: 61-80.
- Johnston, M.J.S., 2009. Near-field earthquake source mechanics at 3.6 km depth, Tau Tona Mine, South Africa, IRIS Seismic Instrumentation Technology Symposium, Palm Springs, CA, USA.
- King, C.-Y., 1986. Gas geochemistry applied to earthquake prediction: An overview. *J. Geophys. Res.*, 91(B12): 12,269-12,281.
- King, C.Y. and Lou, G., 1990. Variations of electric resistance and H₂ and Rn emissions of concrete blocks under increasing uniaxial compression. *Pure Appl. Geophys.*, 134(45-56).
- Kita, I., Matsuo, S. and Wakita, H., 1982. H₂ generation by reaction between H₂O and crushed rock: an experimental study on H₂ degassing from the active fault zone. *J. Geophys. Res.*, 87: 10789-10795.
- Lin, L., Hall, J.A., Lippmann, J., Ward, J., Sherwood-Lollar, B., DeFlaun, M., Rothmel, R., Moser, D.P., Gihring, T.M., Mislowski, B. and Onstott, T.C., 2005. Radiolytic H₂ in continental crust: Nuclear power for deep subsurface microbial communities. *Geochem. Geophys. Geosys.*, 6: Q07003.
- Lippmann-Pipke, J., Sherwood Lollar, B., Niedermann, S., Stroncik, N.A., Naumann, R., van Heerden, E. and Onstott, T.C., 2011. Neon identifies two billion year old fluid component in Kaapvaal Craton. *Chem. Geol.*, 283(3-4): 287-296.
- McGarr, A., Boettcher, M., Fletcher, J.B., Sell, R., Johnston, M.J.S., Durrheim, R., S. Spottiswoode, S. and Milev, A., 2009. Broadband Records of Earthquakes in Deep Gold Mines and a Comparison with Results from SAFOD, California. *Bull. Seism. Soc. Am.*, 99: 2815-2824.
- Mendecki, A.J., 1997. *Seismic Monitoring in Mines*. Chapman and Hall, London, 262 pp.
- Nicolaysen, L.O., 1992. International semi-controlled experiment on seismic events: a review of the background and proposal. *Newsletter, Seismol. Soc. Jpn.*, 3(6): 9-27.
- Nivin, V.A., Belov, N.I., Treloar, P.J. and Timofeyev, V.V., 2001. Relationship between gas geochemistry and release rates and the geomechanical state of igneous rock massifs. *Tectonophysics*, 336: 233-244.
- Pérez, I.A., Sánchez, M.L., García, M.Á. and de Torre, B., 2009. A classification of CO₂ concentrations based on a binary meteorological six variable system. *Agric. Forest Meteorol.*, 149(10): 1686-1692.

- Reches, Z., 2006. Building a Natural Earthquake Laboratory at Focal Depth (DAFSAM-NELSAM Project, South Africa). *Scientific Drilling*, 3: 30-33.
- Sato, M., Sutton, A.J. and McGee, K.A., 1985. Anomalous hydrogen emission from the San Andreas fault observed at the Cienega Winery, Central California. *Pure Appl. Geophys.*, 122: 376-391.
- Seewald, J.S., 2001. Aqueous geochemistry of low molecular weight hydrocarbons at elevated temperatures and pressures: Constraints from mineral buffered laboratory experiments. *Geochim. Cosmochim. Acta*, 65: 1641-1664.
- Sherwood Lollar, B., Frapre, S.K., Weise, S.M., Fritz, P., Macko, S.A. and Welhan, J.A., 1993. Abiogenic methanogenesis in crystalline rocks. *Geochim. Cosmochim. Acta*, 57: 5087-5097.
- Sherwood Lollar, B., Lacrampe-Couloume, G., Slater, G.F., Ward, J., Moser, D.P., Gihring, T.M., Lin, L.H. and Onstott, T.C., 2006. Unravelling abiogenic and biogenic sources of methane in the Earth's deep subsurface. *Chem. Geol.*, 226(3-4): 328-339.
- Sherwood Lollar, B., Lacrampe-Couloume, G., Voglesonger, K., Onstott, T.C., Pratt, L.M. and Slater, G.F., 2008. Isotopic signatures of CH₄ and higher hydrocarbon gases from Precambrian Shield sites: A model for abiogenic polymerization of hydrocarbons. *Geochim. Cosmochim. Acta*, 72(19): 4778-4795.
- Sherwood Lollar, B., Westgate, T.D., Ward, J.A., Slater, G.F. and Lacrampe-Couloume, G., 2002. Abiogenic formation of alkanes in the Earth's crust as a minor source for global hydrocarbon reservoirs. *Nature*, 416(6880): 522-524.
- Stevens, T.O. and McKinley, J.P., 2000. Abiotic controls on H₂ production from basalt-water reactions for aquifer biochemistry. *Environ. Sci. Technol.*, 34: 826-831.
- Sugisaki, R., Ido, M., Takeda, H., Isobe, Y., Hajashi, Y., Nakamura, N., Satake, H. and Mizutani, Y., 1983. Origin of hydrogen and carbon dioxide in fault gases and its relation to fault activity. *J. Geol.*, 91: 23-258.
- Torgersen, T. and Clark, J., 1985. Helium accumulation in groundwater (I): An evaluation of sources and the continental flux of crustal ⁴He in the Great Artesian Basin, Australia. *Geochim. Cosmochim. Acta*, 49: 1211-1218.
- Toutain, J.P. and Baubron, J.C., 1999. Gas geochemistry and seismotectonics: a review. *Tectonophysics*, 304: 1-27.
- Ward, J.A., Slater, G.F., Moser, D.P., Lin, L.-H., Lacrampe-Couloume, G., Bonin, A.S., Davidson, M., Hall, J.A., Mislouack, B., Bellamy, R.E.S., Onstott, T.C. and Sherwood Lollar, B., 2004. Microbial hydrocarbon gases in the Witwatersrand Basin, South Africa: Implications for the deep biosphere. *Geochim. Cosmochim. Acta*, 68(15): 3239-3250.
- Wiersberg, T. and Erzinger, J., 2008. On the origin and spatial distribution of gas at seismogenic depths of the San Andreas Fault from drill mud gas analysis. *Appl. Geochem.*, 23(6): 1675-1690.

Technical Annex

A1 Details on the gas analytical system

A 1.1 First gas analytical setup

A custom made tropicalized climate chamber (Figure 2, ST Gebäudetechnik GmbH, <http://www.stgebaeudetechnik.de>, length: 1.9 m, heights: 1.2 m, widths: 0.9 m) successfully passed a multi-day test in the GFZ climate chamber (40°C, 100% humidity) and proved to effectively transport about 1000 W heat from inside to the surrounding environment while providing laboratory conditions (< 15°C, low humidity) for the enclosed measurement units (pumps, cold trap, QMS, PC, temperature sensor and data logger), see Figure 3. The heat exchange unit is located at the outer side of the box and shielded against shock and dust by a steel panel. Four rolls allow easy handling on unruffled ground. Cased connector plugs enable the communication with the internal systems (PC, data logger and borehole temperature sensor, drainage system, power supply). The lid of the box is kept closed except for maintenance purposes. A pump withdraws borehole gas at a constant rate (2 L h⁻¹) controlled by an Aalborg flowmeter (5-100 ml min⁻¹). Prior to the gas transfer into the QMS the humidity is allowed to condensate in a 100 ml cold trap. The QMS is set to analyse N₂, O₂, ^{40,36}Ar, CH₄, CO₂, H₂ and He and was calibrated with air and certified check gases. The gas component measurement is controlled by the Quadstar software (32-bit, installed on a Windows based PC), which balances all analyzed gas components to 100%. The precision of the gas component analysis amounts to below 2% of the readings. All selected gas components are analysed on a minute-by-minute basis and stored on PC.

A 1.2 Final gas analytical setup

The final realisation of the gas analytical system (Figure 4) was designed to be far more robust under the harsh underground conditions. In particular, it was designed to operate under ambient conditions (temperature, humidity), without PC (data loggers instead), with a considerably reduced dead gas volume and with linear pumps without internal rotating parts (SMG4, Gardner Denver Thomas GmbH). This became possible as the QMS was replaced by gas sensitive sensors for H₂, O₂ (Xgard Crowcon, Type 1, 0 – 2000 ppmv H₂, 0 – 25 vol.% O₂) and CO₂ (Li-COR, Li-820, 150 – 1150 mbar pressure compensated infrared detector with a 14 cm cuvette) to the disadvantage of the analysis of N₂, Ar, CH₄ and He. The overall system fits into two portable cases (Peli 1600 case, 50 x 60 x 23 cm, Peli Products SA), another major improvement compared to the QMS based system. The precision of the gas sensitive sensors amounts to < 3% of the reading for CO₂, H₂ and O₂. With regard to peak height over daily baseline ratios of only about 2-3%, the particular advantage of online measurements needs to be emphasized. Still, due to our continuous monitoring devices the timing of peaks, their heights and shapes are most

clearly recognizable. In contrast to off-line data sets, where the significance of a feature would require a higher precision. The gas composition is analysed on a minute-by-minute basis and stored on a data logger.

A 2 Timeline of the analytical system performances

Since mid January 2007 the borehole gas components N_2 , O_2 , $^{40,36}Ar$, CH_4 , CO_2 , H_2 and He, the borehole temperature and the cubby air pressure are detected and recorded on a minute-by-minute basis (Figure 5). Elected gas flasks were filled with borehole gas for off-line noble gas isotope analysis. After only three weeks the first technical problems interrupted the time series. These problems were related to repeated power cuts, water clogged flow meters and a first QMS filament burn through. A second data series retrieved within a four week interval in March/April 2007 ended due to water clogged flow meters followed by the spare filament burn through. For filament replacements, the QMS was transported to the surface. From December 2007 through April 2008 the QMS was installed again on site, but besides repeated attempts of proper calibration and filament switching the data quality was low in comparison to the 2007 and the later 2009 data and will therefore not be discussed here. Since mid-February 2009 the gas specific sensors (O_2 , CO_2 and H_2) provided high quality borehole gas data until mid-May 2009, when a fatal pump failure ended two months of excellent data retrieval. Unfortunately, data from three weeks during that two-month interval were lost due to a data storage problem. The scheduled repair of the broken pump was shifted from November 2009 into early 2010 due to a two-month closure of the mine for shaft maintenance. After the replacement of the pump and the PC (in favour of a data logger), the removal of the air conditioned box and the cold traps, the final realization of the gas analytical system (March 2010) allowed for a two day cubby air monitoring preceding a six month period of uninterrupted borehole gas monitoring of unprecedented quality.

Figures

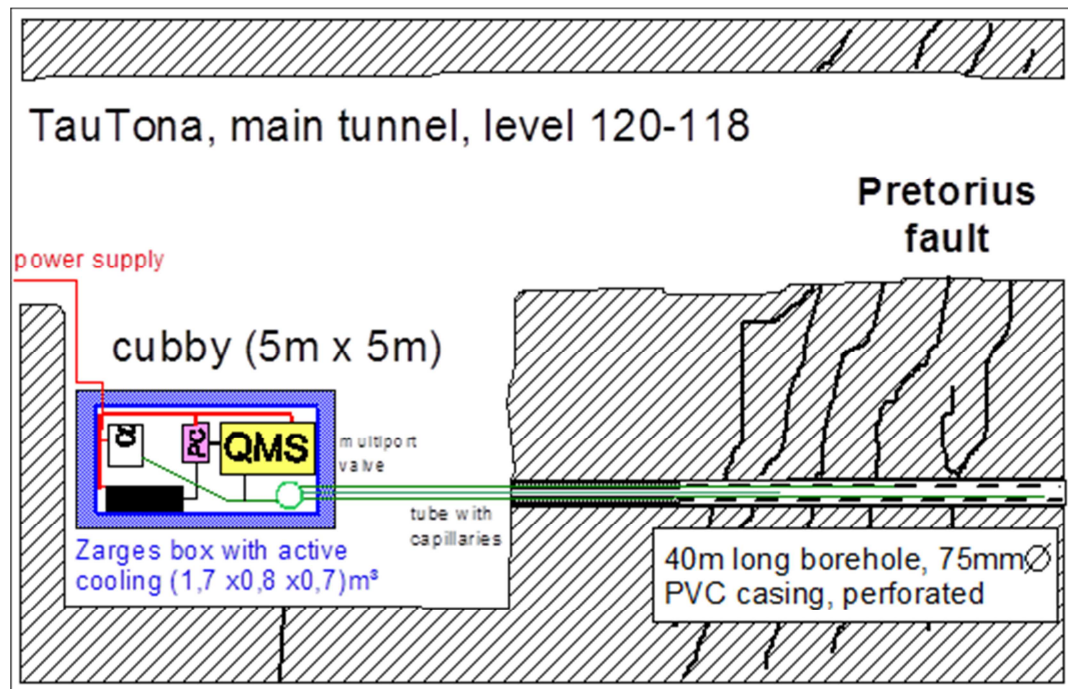


Figure 1: Conceptual sketch of the secure storage of the DAFGAS analytical unit

In the framework of the DAFSAM-NESLAM project five boreholes were drilled. Boreholes DAF1 and DAF2 are interconnected by a 110 m long cross-fault strainmeter, the longest and deepest in the world (Johnston, 2009). Borehole DAF4 was particularly drilled for the need of our real-time gas monitoring project DAFGAS, is 42 m long and rises 25° upwards to allow water to get drained. A plastic tube with an outer diameter of 2 cm is stretched out inside the borehole and acts as a protector for a set of six stainless steel capillaries and cables for three temperature sensors. The capillaries (1/16") reach 20, 30 and 40 meters deep into the borehole) and end in a multiport valve. Gas is withdrawn only through on capillary at a time.



Figure 2: Edgewise and top view of the first set-up of the DAFGAS analytical unit. Main components inside the water vapour tight and air conditioned box are the mass spectrometer with a PC, a pump and a data logger. For details see the technical annex, section A 1.1.

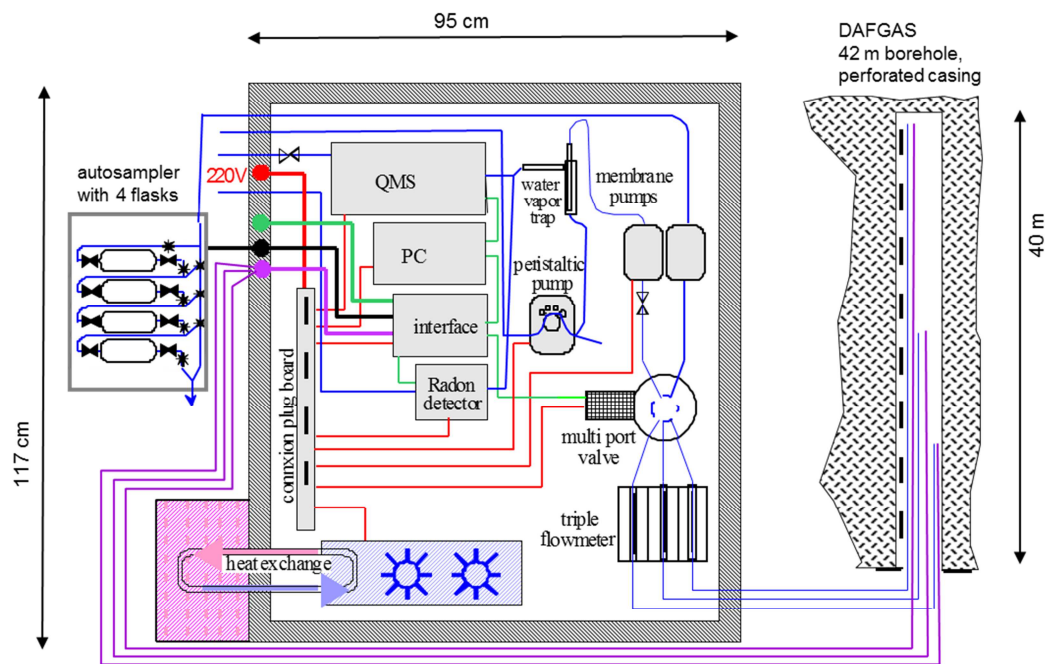


Figure 3: Schematic diagram of the first set-up of the gas analytical unit

Three capillaries and temperature sensors stretch out 20, 30 and 40 m deep into the 42 m long DAFGAS borehole (right hand side). Per default, borehole gas is pumped from the 40 m capillary at a constant rate of 2 L h^{-1} . Inside the water vapour tight and air conditioned box the borehole gas passes through a 100 mL cold trap and enters the mass spectrometer for gas compositional analysis. A data logger stores borehole temperature and cubby temperature and air pressure data. For offline noble gas isotope analysis, 250 mL glass flasks are permanently flushed with the gases at the outlet. For details see the technical annex, section A 1.1.

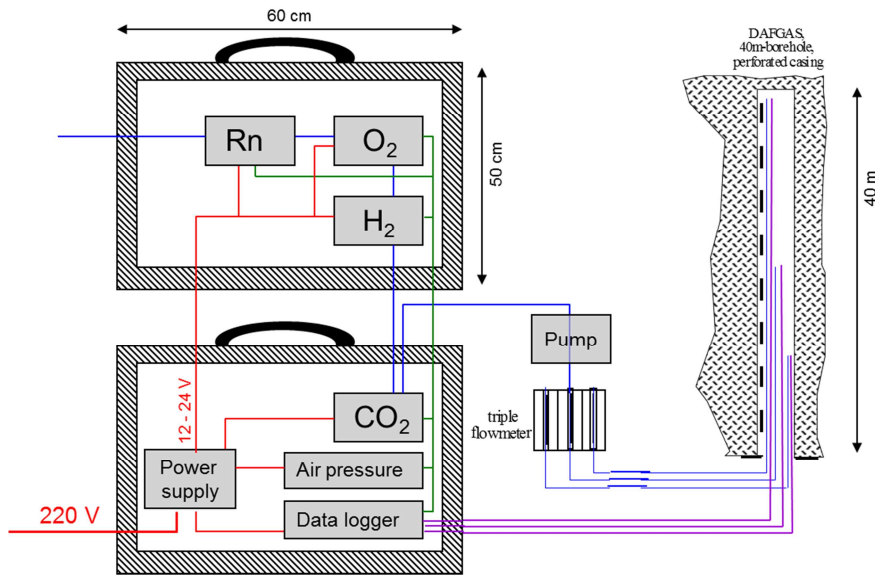


Figure 4: Schematic diagram of final set-up of the gas analytical unit

Three capillaries and temperature sensors stretch out 20, 30 and 40 m deep into the 42 m long DAFGAS borehole (right hand side). Per default, borehole gas is pumped from the 40 m capillary at a constant rate of 2 L h⁻¹ into the three serially-arranged gas specific sensors (CO₂, H₂, O₂) and a ²²²Rn detector. Temperature, air pressure and gas concentrations are stored on a data logger. For offline noble gas isotope analysis, 250 mL glass flasks are permanently flushed with the gases at the outlet. For details see the technical annex, section A 1.2.

	2007												2008												2009												2010								
	1	2	3	4	5	6	7	8	9	10	11	12	1	2	3	4	5	6	7	8	9	10	11	12	1	2	3	4	5	6	7	8	9	10	11	12	1	2	3	4	5	6	7	8	9
DAFGAS data	[Good quality gas data / good quality seismic data from ISSI]												[Good quality gas data / good quality seismic data from ISSI]												[Good quality gas data / good quality seismic data from ISSI]												[Excellent quality gas data / excellent quality seismic data from ISSI and NELSAM]								
seismic data	[Good quality seismic data from ISSI]												[Good quality seismic data from ISSI]												[Good quality seismic data from ISSI]												[Excellent quality seismic data from ISSI and NELSAM]								
Availability of gas / seismic data																																													
no gas data / no seismic data																																													
low quality gas data																																													
good quality gas data / good quality seismic data from ISSI																																													
excellent quality gas data / excellent quality seismic data from ISSI and NELSAM																																													

Figure 5: Timeline of the analytical system performances

Performance of the gas analytical system throughout the years compared to the performance (and availability) of seismic data. For details see the technical annex, section A 2.

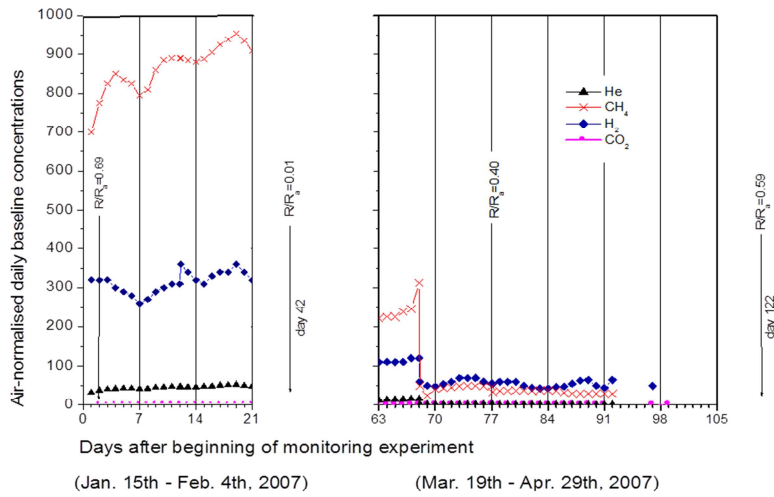


Figure 6: Air normalised daily baseline concentrations

During the first 21 days of the monitoring experiment the air normalised daily baseline geogases concentrations in the borehole gas increased (CH₄ and He) or stayed constant at relatively high levels (H₂ and CO₂). Consistently, the R/R_a value decreased from 0.69 (day 3) to 0.01 (day 42) indicating the significant increase of radiogenic ⁴He in the borehole gas. A final gas breakthrough of tunnel air on day 68 caused a significant reduction of all geogas concentrations in the borehole. Since, the R/R_a value levels around 0.40 – 0.59.

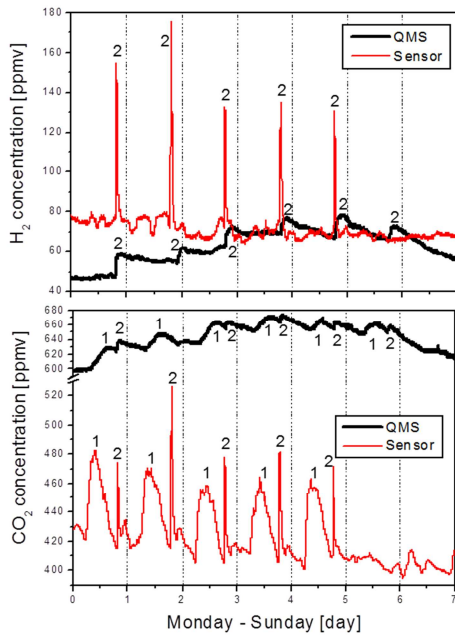


Figure 7: Comparison of H₂ and CO₂ data analysed with the QMS- (first set-up) and the sensor-based analytical systems (final set-up) H₂ and CO₂ concentrations analysed with the QMS in the borehole gas (26.03.-01.04.2007, days 64-70) are compared with those analysed with the sensor based system (17.-24.05.2010, days 1219-1225). Number “1” indicates the broad CO₂ mid-day peak, “2” the afternoon geogas peaks. For further details, see 4.1.3 Technical improvements regarding gas analysis

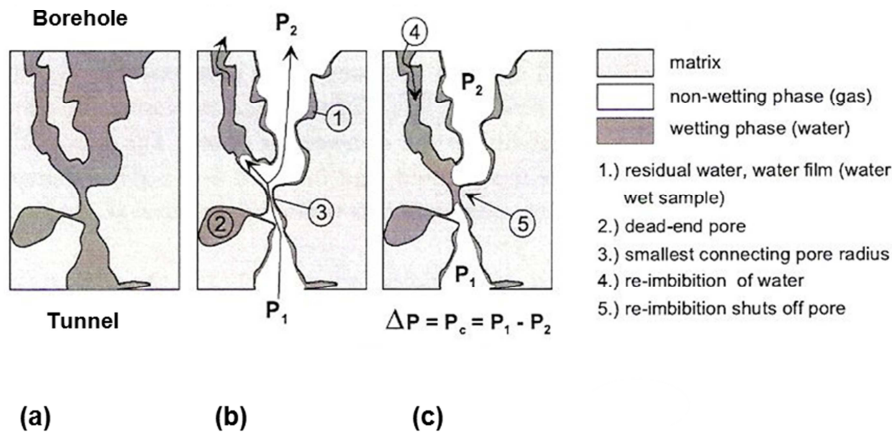


Figure 8: Strip cartoon of gas breakthrough initially water saturated fractures

(a) Initially water saturated fractures are not permeable to advective gas flow, (b) sporadic gas breakthrough is possible as soon as the pressure difference ΔP between the borehole and the tunnel exceeds the capillary pressure threshold $P_{c, \text{threshold}}$ (c) re-clogging by water due to surface tensions; (Hildenbrand et al., 2004)

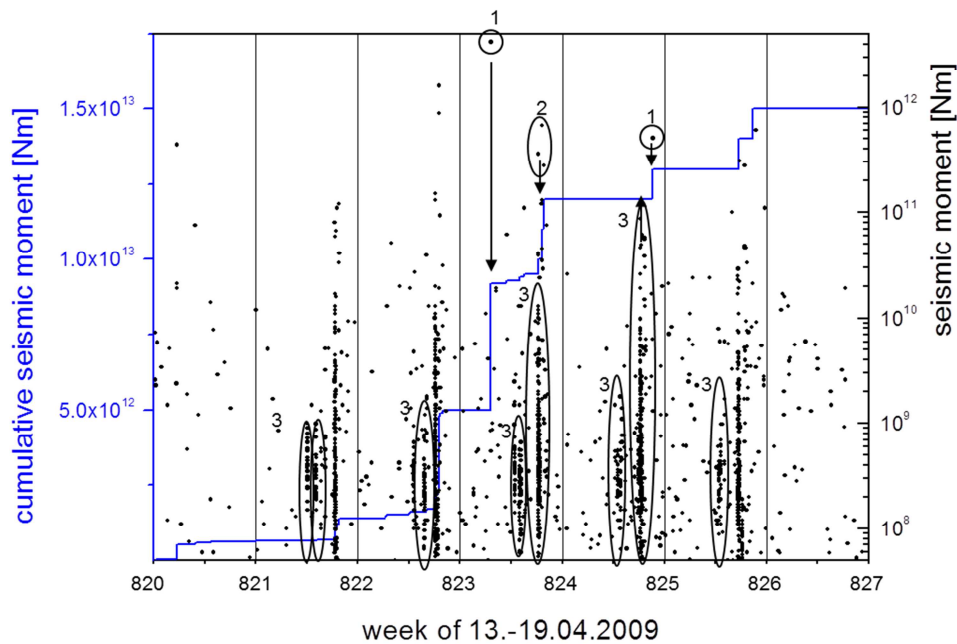


Figure 9: Seismic moment and cumulative seismic moment versus time

Seismic moment (right axis) and cumulative seismic moment (left axis) versus the course of one week, 13th through April 19th 2009. Far distant seismic events (leftist "1", ~1 km) do significantly increase the calculated cumulative seismic moment, but have no effect on the borehole gas composition (not shown). Nearby seismic events with $\geq 1 \cdot 10^{11}$ Nm ("2" and rightist "1") effect the calculated cumulative seismic moments do sometimes effect the borehole gas composition (event "2", but not so the rightist "1"). Some seismic clusters with $\leq 1 \cdot 10^{11}$ Nm hardly effecting the cumulative seismic moment ("3") but still can have a significant effect on the borehole gas composition (Figures 10, top and centre, notice the multiple geogas peaks per day).

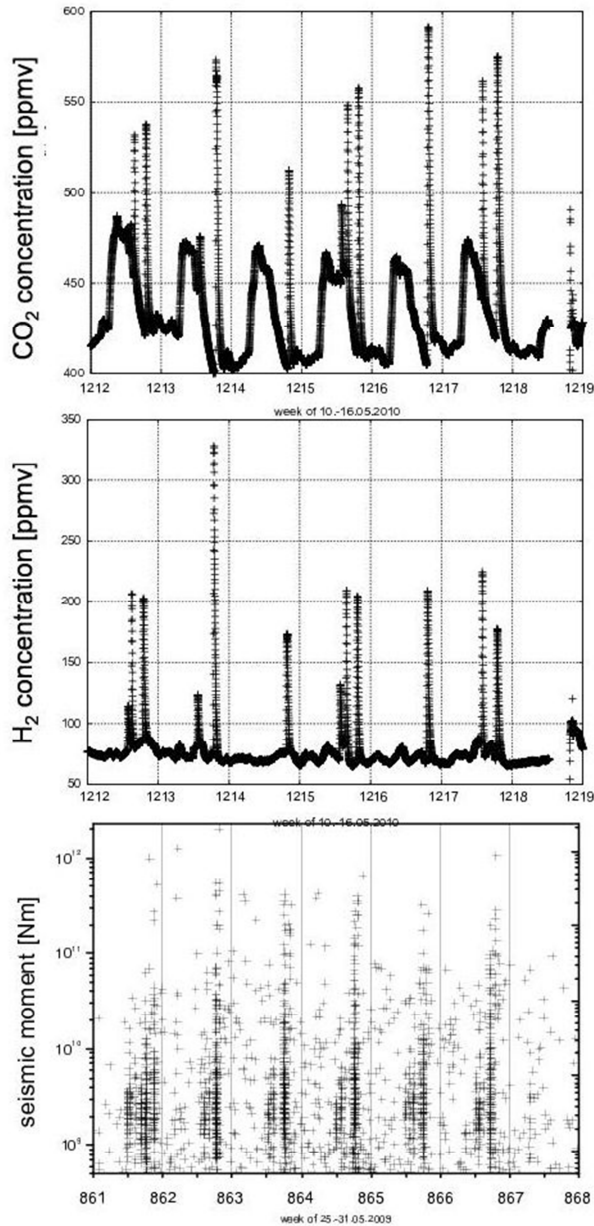


Figure 10: CO_2 and H_2 data and seismic moments versus time
 CO_2 (top) and H_2 concentrations (centre) in the borehole gas between May, 10th through 16th 2010 analysed with the gas sensitive sensors compared to high quality data from a typical week in 2009 (bottom). Besides the broad mid-day CO_2 peak, all other H_2 and CO_2 peaks are quite sharp indicating the high quality of the gas data set. In principle the H_2 and CO_2 peaks correlate with observed multiple clusters of blast induced seismicity (different weeks). We interpret the blast related geogas concentration peaks as due to enhanced gas permeability of the fractures of above $5 \cdot 10^{10} \text{ m}^{-2}$ during times of increased seismicity ($\geq 1 \cdot 10^9 \text{ Nm}$).

Table captions:

Table 1: Overview about four observation periods in respect to the long-term, weekly and daily geogas systematic in the DAFGAS borehole. In the table “1, 2 or 3” denote the number of the sharp geogas peaks, “0” the identification of no such peak while no number indicates that no measurement result is available for the respective day. The solid framed baseline concentration values mark those of March 24th, 2007 at which the final tunnel air breakthrough was observed; “x” indicates data loss due to technical reasons, for further details, see text.

Sample	sampling date	day-ID	^4He ppmv	$^3\text{He}/^4\text{He}$ [10^{-6}]	R/R _a	$^4\text{He}/^{40}\text{Ar}$ [10^{-3}]	$^{40}\text{Ar}/^{36}\text{Ar}$	
<i>Air</i>			5.24	136	1	0.563	295.5	
<i>Borehole gas</i>								
flask #1	17.01.2007	3	12.2 ± 0.7	94 ± 4	0.69	1.2 ± 0.1	294.9 ± 1.1	
flask #2	26.02.2007	43	947.1 ± 67.1	2 ± 1	0.01	16,469 ± 1427	299.6 ± 2.9	
flask #3	02.04.2007	78	21.1 ± 1.1	54 ± 3	0.40	359.3 ± 25.4	296.8 ± 2.9	
flask #4	14.05.2007	120	14.1 ± 0.7	80 ± 6	0.59	70.8 ± 5.0	293.8 ± 1.7	
			[10^{-6}]	[10^{-6}]		[10^{-3}]		
			$\text{cm}^3 \text{g}^{-1} \text{rock}$					
<i>Pore water, DAFBIO drill core</i>								
TT118-BR1	31.01.06		14.1 ± 1.4	0.9 ± 0.4	0.01	16,400,000 ± 100%	481 ± 100%	
<i>Fluid inclusions, DAFBIO drill core</i>								
TT118-BR1	31.01.06		49.2 ± 4.6	1.1 ± 0.2	0.01	11,707 ± 1812	23,300 ± 360	
<i>Fluid inclusions, vein quartz</i>								
MP104-VQ1	16.09.02		66.7 ± 11.3	1.5 ± 0.1	0.01	9,954 ± 2082	111,200 ± 66,980	
MP104-VQ2	16.09.02		23.6 ± 2.6	1.4 ± 0.3	0.01	2,521 ± 470	276,800 ± 52,900	

Table 2: Noble gas concentrations and isotopic compositions from air and from four borehole gas off-line samples (flask #1-4), from a pore water sample of a freshly collected drill core (DAFBIO borehole, TT118-BR1), from its fluid inclusions and from vein quartz samples (Mponeng mine, MP104-VQ1 and -VQ2 (Lippmann-Pipke et al., 2011)). The fluids dissolved in the pore water were allowed to degas into their vacuum tight sampling container during four month storage. Values in *italic* indicate that fractionation must have occurred during this degassing of this low porosity rock ($n = 0.16$, determined by He-porosimetry by Core Petrophysics Inc. (Houston, Texas, USA) on a 1" diameter subcore) and caused the unrealistic high $^4\text{He}/^{40}\text{Ar}$ and the unrealistic low $^{40}\text{Ar}/^{36}\text{Ar}$ values.